
Bidirectional Soft Actor-Critic: Leveraging Forward and Reverse KL Divergence for Efficient Reinforcement Learning

Yixian Zhang, Huaze Tang, Changxu Wei, Wenbo Ding
Tsinghua University

Abstract

The Soft Actor-Critic (SAC) algorithm, a state-of-the-art method in maximum entropy reinforcement learning, traditionally relies on minimizing reverse Kullback-Leibler (KL) divergence for policy updates. However, this approach leads to an intractable optimal projection policy, necessitating gradient-based approximations that can suffer from instability and poor sample efficiency. This paper investigates the alternative use of forward KL divergence within SAC. We demonstrate that for Gaussian policies, forward KL divergence yields an explicit optimal projection policy—corresponding to the mean and variance of the target Boltzmann distribution’s action marginals. Building on the distinct advantages of both KL directions, we propose Bidirectional SAC, an algorithm that first initializes the policy using the explicit forward KL projection and then refines it by optimizing the reverse KL divergence. Comprehensive experiments on continuous control benchmarks show that Bidirectional SAC significantly outperforms standard SAC and other baselines, achieving up to a 30% increase in episodic rewards, alongside enhanced sample efficiency.

1 Introduction

Maximum entropy reinforcement learning has emerged as a powerful framework for tackling complex decision-making problems, including mobile robot control [de Jesus et al., 2021], autonomous driving [Yang et al., 2024], and protein engineering [Wang et al., 2023]. The Soft Actor-Critic (SAC) algorithm [Haarnoja et al., 2018a], a prominent algorithm within this framework, has demonstrated superior performance across a variety of continuous benchmark tasks. In SAC, the optimization of the policy is achieved by seeking a projection policy with respect to the Boltzmann distribution based on the Q-function, where the reverse Kullback-Leibler (KL) divergence is used as the probabilistic measure. However, due to the intractability of the projection policy, gradient-based methods are employed to iteratively adjust the parameterized policy towards the optimal projection [Haarnoja et al., 2018b]. Despite their utility, these optimization techniques can exhibit instability and require a substantial number of samples to achieve convergence [Chan et al., 2022, Banerjee et al., 2022]. In fact, even in the simple case of a Gaussian distribution, we observe that gradient optimization methods often fail to converge.

The use of reverse KL divergence as a measurement to guide policy projection has two key advantages, as outlined in prior studies [Haarnoja et al., 2018b, Duan et al., 2021b, Hu et al., 2025]: First, minimizing the reverse KL divergence ensures that the expected Q-function value of the updated policy is greater than that of the previous policy. Second, the gradient of the reverse KL divergence is computationally tractable, avoiding the need for the intractable normalization term in the Boltzmann distribution. However, if the reverse KL divergence optimization becomes unstable, such as when the KL divergence increases during gradient optimization, these advantages are lost. An alternative approach involves the forward KL divergence, which is commonly utilized in variational policy

optimization [Dayan and Hinton, 1997, Toussaint and Storkey, 2006], where few papers concentrate on its use in the SAC algorithm.

In this paper, we find that, by replacing the reverse KL divergence with the forward KL divergence in the SAC framework, denoted as Forward SAC, the optimal projection policy becomes explicit. Specifically, for Gaussian policies—widely used in stochastic continuous actor-critic algorithms [Haarnoja et al., 2018a, Schulman et al., 2017, Mnih et al., 2016, Schulman et al., 2015]—the optimal projection policy within forward KL divergence corresponds to the mean and variance of the action under the Boltzmann distribution. This insight allows us to directly compute the optimal projection policy using numerical integration, thereby achieving stable and sample-efficient policy updating. However, it is not guaranteed that the updated policy within forward KL divergence can maximize the expected Q value. These characteristics of the two directions of KL divergence lead to a direct idea: Can we integrate the advantages of these two directions of KL divergence? Therefore, we propose the Bidirectional SAC algorithm, which uses the optimal projection policy in forward KL divergence as the initialization policy, and it optimizes the policy by minimizing the reverse KL divergence. To efficiently compute the mean and variance, we adapt the Value Decomposition Networks (VDN) [Sunehag et al., 2017], originally designed for multi-agent reinforcement learning, into the single-agent context for Q-function learning, where we denote it as VDN-a networks. Our theoretical analysis, grounded in Copula theory, elucidates how the VDN-a architecture is designed to approximate the necessary marginal properties of the Boltzmann distribution. Supported by experimental results, this approach facilitates the efficient learning required for the independent numerical integration of the mean and variance for each action dimension. Comparative experiments in MuJoCo and Box2D environments [Todorov et al., 2012, Catto, 2011] demonstrate that the Bidirectional SAC algorithm outperforms the SAC algorithm and other baseline methods, achieving up to 30% increase in episodic rewards.

Our contributions are as follows:

- We introduce the Forward SAC algorithm, in which the updated policy is the optimal projection to the Boltzmann distribution of the Q-function.
- We conduct a thorough analysis for the use of forward and reverse KL divergence in the SAC algorithm, where we find that the use of both directions has its advantages and disadvantages. To leverage these advantages, we propose the Bidirectional SAC algorithm, which optimizes the policy sample efficiently.
- To efficiently compute the optimal projection, we propose VDN-a networks for single-agent Q-function learning. Our theoretical analysis and experimental results demonstrate its efficacy in approximating the marginals of the Boltzmann distribution, crucial for efficiently computing the forward KL optimal projection within Bidirectional SAC. Our experiments demonstrate that the Bidirectional SAC algorithm converges rapidly and outperforms baseline algorithms, achieving up to 30% increase in episodic rewards.

2 Preliminaries and background

In this section, we briefly introduce the maximum entropy reinforcement learning and the famous soft actor-critic (SAC) algorithm [Haarnoja et al., 2018a].

2.1 Maximum entropy reinforcement learning

We consider policy search in an infinite-horizon Markov decision process $\langle \mathcal{S}, \mathcal{A}, p, r, \rho \rangle$, with continuous state \mathcal{S} and action \mathcal{A} space. The transition function $p : \mathcal{S} \times \mathcal{A} \times \mathcal{S} \rightarrow [0, \infty)$ defines the probability density of transitioning, and rewards are $r_t = r(s_t, a_t) \in [r_{\min}, r_{\max}]$.

The objective of reinforcement learning is to learn an optimal policy π^* that maximizes the cumulative expected rewards $\pi^* = \arg \max_{\pi} \mathbb{E}_{\tau \sim \pi} [\sum_{l=t}^{\infty} r_l]$, where τ denotes the trajectory under policy π originating at (s_t, a_t) [Sutton and Barto, 2018]. The maximum entropy reinforcement learning extends the standard objective by incorporating an entropy term $\mathcal{H}(\pi(\cdot | s)) = -\mathbb{E}_{a \sim \pi(\cdot | s)} [\log \pi(a | s)]$, thereby encouraging policies to maintain stochasticity and explore more effectively. In this setting, the optimal policy π_{Ent}^* seeks to maximize both the expected cumulative rewards and the entropy of

the policy at each state [Haarnoja et al., 2018b]:

$$\pi_{\text{Ent}}^* = \arg \max_{\pi} \mathbb{E}_{\tau \sim \pi} \left[\sum_{l=t} r_l + \alpha \mathcal{H}(\pi(\cdot | s_l)) \right], \quad (1)$$

where α is the temperature parameter to determine the relative importance of entropy and reward.

2.2 Soft actor-critic

Equation (1) is addressed by various methods [Ziebart et al., 2008, Abdolmaleki et al., 2018a, Kim et al., 2024]. Soft Q-Learning (SQL) [Haarnoja et al., 2017], an early Q-learning approach, used an approximate sampler for the actor, limited by posterior approximation accuracy. To overcome this limitation, the Soft Actor-Critic (SAC) algorithm is introduced [Haarnoja et al., 2018a], where the actor is parameterized within a predefined policy class. In the SAC algorithm, the soft Q-function under policy π is defined as:

$$Q^{\pi}(s_t, a_t) = r_t + \mathbb{E}_{\tau \sim \pi} \left[\sum_{l=t+1} (r_l + \alpha \mathcal{H}(\pi(\cdot | s_l))) \right],$$

The policy in SAC is typically modeled using a parameterized family of distributions, often instantiated as a multivariate Gaussian distribution family Π [Yang et al., 2021, Ziesche and Rozo, 2024], to enable efficient exploration and exploitation. In the update process, the soft Q-function and Gaussian policy are typically parameterized by neural networks $Q_{\theta}(s_t, a_t)$ and $\pi_{\phi}(a_t | s_t)$, respectively, where $a_t \sim \mathcal{N}(f_{\phi}(s_t), \Sigma_{\phi})$. Parameters of these neural networks are denoted as θ and ϕ . The soft Q-function is updated with [Haarnoja et al., 2018b]:

$$\nabla_{\theta} J_Q(\theta) = \nabla_{\theta} Q_{\theta}(s_t, a_t) [Q_{\theta}(s_t, a_t) - (r_t + Q_{\bar{\theta}}(s_{t+1}, a_{t+1}) - \alpha \log \pi_{\phi}(a_{t+1} | s_{t+1}))], \quad (2)$$

where $Q_{\bar{\theta}}(s_{t+1}, a_{t+1})$ represents the target soft Q-function with parameters $\bar{\theta}$, which are updated periodically to stabilize training [Mnih et al., 2015]. The policy is optimized by the soft policy improvement, which projects the Boltzmann distribution $q(\cdot | s_t) = \frac{\exp(\frac{1}{\alpha} Q^{\pi_{\text{old}}}(s_t, \cdot))}{Z^{\pi_{\text{old}}}(s_t)}$ onto the Gaussian distribution family through minimization of the reverse Kullback-Leibler (KL) divergence $D_{\text{KL}}(\pi || q)$:

$$\pi_{\text{new-r}} = \arg \min_{\pi' \in \Pi} D_{\text{KL}} \left(\pi'(\cdot | s_t) \left\| \frac{\exp(\frac{1}{\alpha} Q^{\pi_{\text{old}}}(s_t, \cdot))}{Z^{\pi_{\text{old}}}(s_t)} \right\| \right), \quad (3)$$

where the partition function $Z^{\pi_{\text{old}}}(s_t) = \int_{\mathcal{A}} \exp(\frac{1}{\alpha} Q^{\pi_{\text{old}}}(s_t, a)) da$ ensures that the distribution is normalized. In practice, policy parameters are typically updated using stochastic gradient descent, where an approximated projection policy $\tilde{\pi}_{\text{new-r}}$ is computed as:

$$\tilde{\pi}_{\text{new-r}} = \pi_{\text{old}} - \beta \nabla_{\phi} J_{\pi}(\phi), \quad (4)$$

with the gradient update given by $\nabla_{\phi} J_{\pi}(\phi) = \nabla_{\phi} [\alpha \log \pi_{\phi}(a_t | s_t) - Q_{\theta}(s_t, a_t)]$, where a_t is implicitly parameterized by ϕ through $a_t \sim \mathcal{N}(f_{\phi}(s_t), \Sigma_{\phi})$, and β denotes the learning rate. This updating rule directs the new policy $\tilde{\pi}_{\text{new-r}}$ towards the true projection $\pi_{\text{new-r}}$, but the resulting policy often remains some distance away from the true projection itself. Nevertheless, this approach is widely used in prominent SAC-based algorithms, including conservative Q-Learning [Kumar et al., 2020], inverse soft Q-Learning [Garg et al., 2021], and distributional soft actor-critic [Duan et al., 2021a], among others. However, applying gradient descent to optimize the reverse KL divergence can suffer from instability and inefficiency, largely attributable to its pathological curvature [Chan et al., 2022]. Our theoretical analysis and empirical findings indicate that this optimization approach frequently yields optimized distributions that deviate significantly from the true target distribution, even when applied in relatively simple scenarios.

In contrast to the reverse KL divergence traditionally employed in SAC, the forward KL divergence $D_{\text{KL}}(q || \pi')$ has been extensively investigated in alternative reinforcement learning frameworks, including variational policy optimization [Abdolmaleki et al., 2018b, Song et al., 2020, Abdolmaleki et al., 2017]. These methodologies present a fundamentally different perspective on policy optimization and have demonstrated comparable or superior performance across various benchmark environments [Fellows et al., 2019, Liu et al., 2022]. Despite these promising results, a systematic examination of the utilization and comparative efficacy of different KL divergence directions within

the SAC framework remains notably absent from the literature. Our work addresses this critical research gap by rigorously analyzing the standard SAC algorithm and methodically exploring the integration of forward KL divergence within this framework. This investigation ultimately leads to our proposed Bidirectional SAC algorithm, which strategically combines the complementary advantages of both KL divergence directions to enhance sample efficiency and asymptotic performance.

3 Two directions of KL divergence in SAC algorithm

In this section, we show that the use of gradient descent for optimizing reverse KL divergence is unstable, where a single gradient step is hard to decrease the reverse KL divergence even for a simple target distribution. For the use of forward KL divergence in the SAC algorithm, we derive the explicit form of the projection policy in the forward direction of KL divergence, which can be efficiently computed through numerical integration. Ultimately, we introduce a practical way to efficiently estimate numerical integration by using specially designed neural networks.

3.1 Gradient descent in reverse KL divergence

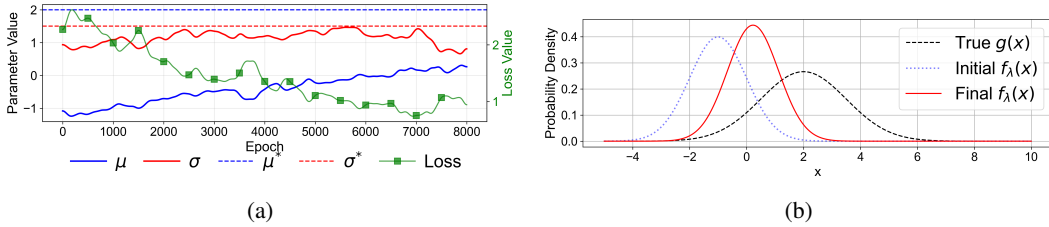


Figure 1: Optimization of the parameterized distribution $f_\lambda(x)$ towards the true distribution $g(x)$ using gradient descent with reverse KL divergence as the loss function. (a) The optimization process with respect to the parameters $\lambda = (\mu, \sigma)$ and the corresponding change in loss function. (b) Comparison of the initial and final distributions after optimization, alongside the true distribution.

To examine the effectiveness of gradient-based methods in minimizing reverse KL divergence, we consider two Gaussian distributions: the true distribution $g(x)$ and a parameterized distribution $f_\lambda(x)$, where $\lambda = (\mu, \sigma)$ represents the mean and standard deviation. The loss function is the reverse KL divergence $D_{\text{KL}}(f_\lambda(x)|g(x))$, and we optimize the parameters λ using gradient descent over 8000 epochs to approximate the true distribution. Let the true distribution $g(x)$ have mean μ^* and standard deviation σ^* . The optimization process is illustrated in Figure 1.

The results show that while the gradient-based optimization method leads to a reduction in the KL divergence loss, it struggles to accurately converge to the optimal parameters μ^* and σ^* , as demonstrated in the distribution comparison on the right side of Figure 1. This behavior can be attributed to the inherent instability of the reverse KL divergence, which depends on samples drawn from the distribution to be optimized. Such instability has been shown to slow down the convergence process [Chan et al., 2022, Kobayashi, 2022]. Therefore, methods that directly target the true distribution may offer more efficient learning. In the following subsection, we demonstrate that employing the forward KL divergence, which learns directly from the mean and variance of the true distribution, significantly enhances optimization efficiency.

3.2 The explicit form of the projection policy

Considering the forward KL divergence, reformulating Problem (3) as:

$$\pi_{\text{new-f}} = \arg \min_{\pi' \in \Pi} D_{\text{KL}} \left(q(\cdot | s_t) \parallel \pi'(\cdot | s_t) \right). \quad (5)$$

This optimization problem can be resolved by this key observation: while the covariance matrix in a Gaussian policy π' is theoretically dense, it is commonly approximated as a diagonal matrix for computational simplicity in optimization [Haarnoja et al., 2018a, Raffin et al., 2021, Huang et al., 2022]. Consequently, the n -dimensional multivariate Gaussian distribution simplifies to n independent one-dimensional Gaussian distributions, where the correlations between action dimensions

are implicitly modeled by the neural networks. We begin by refining the optimization objective as follows:

$$D_{\text{KL}} \left(q(\cdot | s_t) \parallel \pi'(a | s_t) \right) = \int_{\mathcal{A}} q(a | s_t) \log q(a | s_t) - q(a | s_t) \log \pi'(a | s_t) da. \quad (6)$$

For convenience, we denote the forward KL divergence as $D_{\text{KL}}(q(\cdot | s_t) \parallel \pi'(a | s_t))$ as D_{KL} for the remainder of this paper. Denoting the dimension of action space \mathcal{A} is N , let $\pi'(a | s_t) = \prod_i^N \pi'_i(a^i | s_t)$, where each $\pi'_i(\cdot | s_t) = \mathcal{N}(f_\phi^i(s_t), \Sigma_\phi^i)$ represents a one-dimensional Gaussian distribution in dimension i , and $f_\phi^i(s_t), \Sigma_\phi^i$ represent the corresponding network output and the standard deviation of the action in dimension i , respectively. We derive the partial derivative with respect to $f_\phi^i(s_t)$ and Σ_ϕ^i in the objective function of Equation (6) as follows:

$$\frac{\partial D_{\text{KL}}}{\partial f_\phi^i(s_t)} = \frac{1}{\Sigma_\phi^i} \int_{\mathcal{A}_i} q_i(a^i) (a^i - f_\phi^i(s_t)) da^i, \quad \frac{\partial D_{\text{KL}}}{\partial \Sigma_\phi^i} = \frac{1}{2\Sigma_\phi^i} - \frac{1}{2(\Sigma_\phi^i)^2} \int_{\mathcal{A}_i} q_i(a^i) (a^i - f_\phi^i(s_t))^2 da^i.$$

Here, $q_i(a^i) = q_i(a^i | s_t)$ represents the marginal distribution of $q(a | s_t)$ with respect to dimension i . The detailed derivations are provided in Appendix A. By setting $\frac{\partial D_{\text{KL}}}{\partial f_\phi^i(s_t)} = 0$ and $\frac{\partial D_{\text{KL}}}{\partial \Sigma_\phi^i} = 0$, we can solve for the optimal solution of Problem (5), yielding the optimal $f^i(s_t)^*$ and Σ^{i*} :

$$f^i(s_t)^* = \int_{\mathcal{A}_i} q_i(a^i | s_t) a^i da^i, \quad \Sigma^{i*} = \int_{\mathcal{A}_i} q_i(a^i | s_t) (a^i - f_\phi^i(s_t))^2 da^i.$$

Thus, the optimal solution to Problem (5) is elegantly expressed in terms of the mean and variance of the marginal distribution of $q(\cdot | s_t)$, offering an explicit projection policy that does not rely on iterative optimization methods such as gradient-based approaches.

3.3 VDN-a network for efficient numerical integration

To compute the optimal values $f^i(s_t)^*$ and Σ^{i*} efficiently, we introduce the VDN-a network as the critic network to learn the marginal Q values $Q_i(s_t, a_t^i)$ for each action dimension a_t^i . This approach is inspired by Value Decomposition Networks (VDN), where a brief introduction to it is provided in Appendix C.1. Similar to VDN, which designs an independent subnetwork for each agent, the VDN-a network treats each action dimension along with the entire state as an individual "agent" and constructs an independent subnetwork for it. The architecture of the VDN-a network is illustrated in Figure 2. Since each action a_t^i is a single-dimensional data point, it is mapped to an embedding e_t^i through a multilayer perceptron (MLP) for complex pattern recognition. These embeddings are then concatenated with the state s_t to form (s_t, e_t^i) , which are fed into the i -th subnetwork to obtain the marginal Q value $Q_i(s_t, a_t^i)$ for action a_t^i . To enhance the learning capacity of the VDN-a network, an auxiliary network is also incorporated. This auxiliary network takes the entire state and action tuple $(s_t, a_t^1, \dots, a_t^N)$ as input and outputs $U(s_t, a_t)$. The outputs of each subnetwork are aggregated by summing them together with the auxiliary network's output to form the final Q value $Q(s_t, a_t)$. Once the marginal Q values are learned, the marginal distributions $q_i(\cdot | s_t)$ are

obtained by $q_i(a_t^i | s_t) = \frac{\exp(\frac{1}{\alpha} Q_i(s_t, a_t^i))}{\int_{\mathcal{A}_i} \exp(\frac{1}{\alpha} Q_i(s_t, a^i)) da^i}$, where \mathcal{A}_i is the i -th dimension of the action space and the integration is performed using numerical integration, as detailed in the Appendix D.1. We also prove in the Appendix C.2 that if the auxiliary network is sufficiently learned or each dimension of the action is independent, the learned $q_i(a_t^i | s_t)$ is actually the true marginal distribution of the $q(\cdot | s_t)$. To compute the optimal values $f^i(s_t)^*$ and Σ^{i*} , only the mean and variance of the marginal distribution $q_i(\cdot | s_t)$ are required. While direct estimation of the complete marginal distribution remains computationally intractable, empirical results demonstrate that the proposed critic network

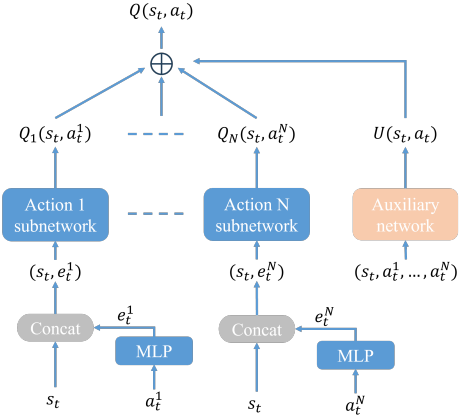


Figure 2: The structure of VDN-a network

architecture effectively captures the first two moments—specifically the mean and variance—of these marginal distributions through numerical integration techniques. The mathematical formulation and implementation details of this integration procedure are presented in Appendix D.1 due to space constraints.

4 The Bidirectional SAC

This section provides a general analysis of the properties of the two directional variants of SAC algorithms. The analysis reveals that each directional variant possesses distinct advantages and disadvantages. Subsequently, we demonstrate that the Bidirectional SAC effectively integrates the strengths of both directional approaches while mitigating their respective limitations.

4.1 Analysis of the use in forward and reverse KL divergence in SAC

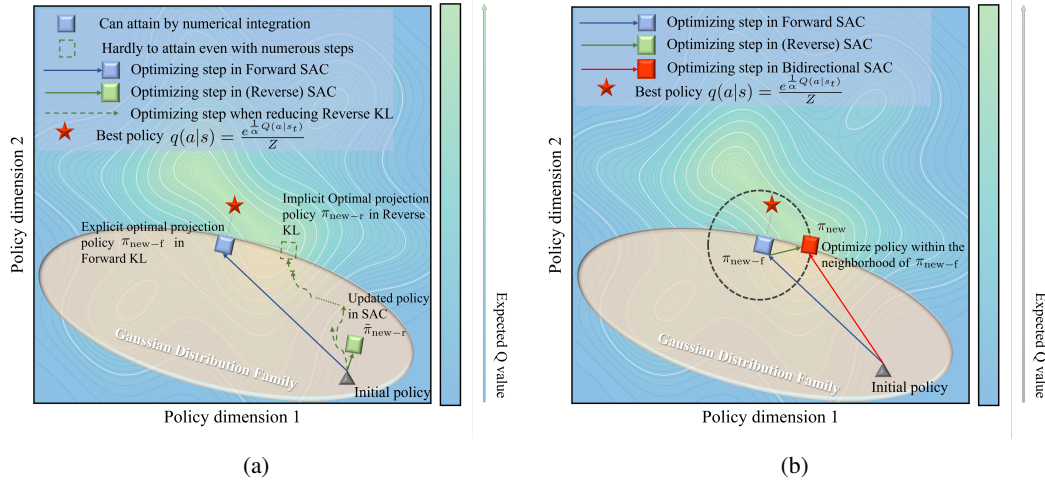


Figure 3: Conceptual illustration of policy optimization dynamics for (Reverse) SAC and Forward SAC. The target Boltzmann distribution is $q(\cdot | s_t)$, and the shaded region represents the Gaussian distribution family for policy π' . (a) Comparison of two directions of KL divergence. (b) The schematic diagram of Bidirectional SAC.

In this section, we contrast the properties of policy updates in the standard SAC algorithm, which minimizes the reverse KL divergence $D_{\text{KL}}(\pi' \| q)$, with our proposed Forward SAC approach, which minimizes the forward KL divergence $D_{\text{KL}}(q \| \pi')$.

Forward SAC This approach optimizes the policy by minimizing the forward KL divergence $D_{\text{KL}}(q(\cdot | s_t) \| \pi'(\cdot | s_t))$, as formulated in Equation (5). As derived in Section 3, the optimal projection policy $\pi_{\text{new-f}}$ within the family Π that minimizes this divergence can be computed explicitly. Specifically, the optimal mean $f^i(s_t)^*$ and variance Σ^{i*} for each action dimension i correspond to the mean and variance of the marginal target distribution $q_i(\cdot | s_t)$, calculable via numerical integration. Thus, the policy $\pi_{\text{new-f}}$ representing the closest projection of $q(\cdot | s_t)$ onto Π in the forward KL sense is directly attainable in each iteration. However, minimizing $D_{\text{KL}}(q \| \pi')$ does not theoretically guarantee that the resulting policy $\pi_{\text{new-f}}$ maximizes the expected Q value $\mathbb{E}_{a \sim \pi_{\text{new-f}}} [Q^{\pi_{\text{new-f}}}(s_t, a)]$ within the policy family Π .

(Reverse) SAC The standard SAC algorithm performs policy improvement by minimizing the reverse KL divergence $D_{\text{KL}}(\pi'(\cdot | s_t) \| q(\cdot | s_t))$, as defined in Equation (3). Due to the intractability of directly solving this minimization, SAC employs stochastic gradient descent on the policy parameters ϕ , using the update rule derived from $J_{\pi}(\phi)$ (approximated in Equation (4)). As established by Haarnoja et al. [2018b], successfully reducing the reverse KL divergence $D_{\text{KL}}(\pi' \| q)$ guarantees an improvement in the policy objective, ensuring that $\mathbb{E}_{a \sim \pi_{\text{new-r}}} [Q^{\pi_{\text{new-r}}}(s_t, a_t)] \geq \mathbb{E}_{a \sim \pi_{\text{old}}} [Q^{\pi_{\text{old}}}(s_t, a_t)]$. This provides a theoretical basis for monotonic policy improvement. However, the practical gradient-based optimization faces significant challenges. As discussed in Section 3

and illustrated in Figure 1, estimating the gradient $\nabla_{\phi} J_{\pi}(\phi)$ requires sampling actions a_t from the current policy $\pi_{\phi}(\cdot | s_t)$. This sampling process often introduces high variance into the gradient estimates, leading to optimization instability and potentially slow or unreliable convergence towards the true projection $\pi_{\text{new-r}}$ [Chan et al., 2022, Kobayashi, 2022]. Figure 3a provides a conceptual visualization of these distinct optimization dynamics within the policy space Π . The optimization target is the Boltzmann distribution $q(\cdot | s_t)$. Both algorithms seek an optimal projection policy within Π . Forward SAC identifies the policy $\pi_{\text{new-f}}$ that is the direct projection of q onto Π with respect to the forward KL divergence. This point is efficiently computed via integration (as shown in our work) but might not coincide with the policy in Π that yields the highest expected Q value. Standard SAC, conversely, takes one updating step based on gradients derived from the reverse KL objective (Equation (4)). While a successful gradient step aims to improve the expected $Q^{\pi_{\text{old}}}$, the practical realization involves noisy updates.

4.2 Bidirectional SAC

It is observed that Forward SAC can find the optimal projection policy $\pi_{\text{new-f}}$ through forward KL divergence, and SAC can perform policy improvement through minimizing reverse KL divergence. Therefore, in every iteration, by setting the initial policy as the optimal projection policy $\pi_{\text{new-f}}$ in Forward SAC and improving it by optimizing the reverse KL divergence within a certain neighborhood of $\pi_{\text{new-f}}$, Bidirectional SAC is proposed. The optimization problem of Bidirectional SAC is derived as:

$$\mathcal{L}(\pi) = D_{\text{KL}} \left(\pi(\cdot | s_t) \parallel q(\cdot | s_t) \right) + \epsilon \left[\|f^i(s_t)^* - f^i(s_t)\|^2 + \|\Sigma^{i*} - \Sigma^i\|^2 \right]. \quad (7)$$

Here, $f^i(s_t)$ and Σ^i denote the mean and variance of the policy π . The optimal projection policy $\pi_{\text{new-f}}$ serves as an initial foundation for the subsequent policy improvement phase. This phase is methodically facilitated through the optimization of reverse KL divergence, as illustrated in Figure 3b. The figure demonstrates how Bidirectional SAC explicitly computes the optimal projection policy, which then functions as a strategic starting point. The resultant updated policy π_{new} is optimized within a neighborhood of this initial policy, with the neighborhood's extent regulated by the hyperparameter ϵ . Through this methodological approach, Bidirectional SAC effectively synthesizes the advantages of optimization in both forward and reverse KL divergence directions.

The optimization process within each step initiates with an initial policy that represents the optimal projection onto the Boltzmann distribution $q(\cdot | s_t)$. Subsequently, the algorithm identifies an enhanced policy through the policy improvement step. To efficiently optimize this objective, we employ an actor network π_{ϕ} trained via the loss function $\mathcal{L}(\pi_{\phi})$. Gradient descent remains our optimization method of choice, implemented by modeling the policy's mean $f_{\phi}^i(s_t)$ and variance Σ_{ϕ}^i using neural networks. This updating procedure demonstrates enhanced sample efficiency and stability, primarily attributable to the utilization of the MSE loss function. The current implementation establishes a robust foundation while opening avenues for future refinements that would more comprehensively leverage the theoretical advantages of the optimal projection policy. This represents a promising direction for extending the framework, as elaborated in Section 6. The complete Bidirectional SAC algorithm is formally presented in Algorithm 1.

Algorithm 1 Bidirectional SAC algorithm

Hyperparameters: Total number of training steps \mathcal{L} , mini-batch size \mathcal{M} , the update epoch \mathcal{J} of neural networks each training, and the learning rate β

- 1: Initialize the critic network Q_{θ} , actor network π_{ϕ} and replay buffer \mathcal{B} .
 - 2: Start with the initial state s_0
 - 3: **for** $l = 1, \dots, \mathcal{L}$ **do**
 - 4: Using policy π_{ϕ} , collect and store transitions (s_t, a_t, r_t, s_{t+1}) in replay buffer \mathcal{B} .
 - 5: **for** $j = 1, \dots, \mathcal{J}$ **do**
 - 6: Sample mini-batch $\{(s_i, a^i, r_i, s_{i+1}) \mid i = 1, \dots, \mathcal{M}\}$ from \mathcal{B} .
 - 7: Update the critic network Q_{θ} by $\theta \leftarrow \theta - \beta \nabla_{\theta} J_Q(\theta)$ in (2)
 - 8: Update the actor parameters with $\phi \leftarrow \phi - \beta \nabla_{\phi} \mathcal{L}(\pi_{\phi})$ in (7).
 - 9: **end for**
 - 10: **end for**
-

5 Experiment result

This section evaluates the episodic reward of Bidirectional SAC, including an ablation study against traditional SAC and Forward SAC. We benchmark performance on several MuJoCo environments [Todorov et al., 2012] (Swimmer, Hopper, Walker2D, Ant, Humanoid, and HumanoidStandup), chosen for their varying complexity and common reinforcement learning objectives such as locomotion and stability [Batra et al., 2024]. Additional results from other MuJoCo and Box2D [Catto, 2011] tasks are in Appendix F.

5.1 Overall performance

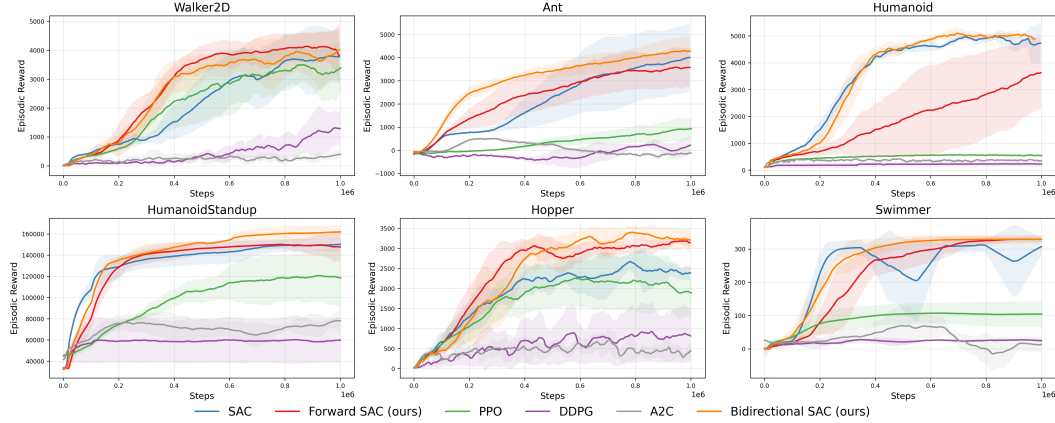


Figure 4: The episodic reward in MuJoCo environments for Bidirectional SAC, Forward SAC, and other benchmarks in the training process.

We compare the performance of the Bidirectional SAC algorithm with the traditional SAC algorithm and Forward SAC algorithm, as well as established benchmarks, including A2C [Wu et al., 2017], PPO [Batra et al., 2024], and DDPG [Lillicrap, 2015]. The results are shown in Figure 4. It is demonstrated in the figure that both Bidirectional SAC and Forward SAC enjoy faster convergence compared to traditional SAC, which is deemed as sample efficient because it converges faster than other benchmarks. Compared to the benchmark algorithms, Forward SAC attains better overall performance in simple and medium complex environments, including Swimmer, Hopper, and Walker2D. However, it can only perform mediocre or even worse in other complex environments. This may be due to that in complex environments, the distribution landscape of Boltzmann distribution $q(\cdot|s_t)$ is too complex that even the optimal policy with respect to Forward KL divergence could cause a substantial difference in the performance of the policy. This issue can be overcome by the Bidirectional SAC algorithm, which searches for better performance policies with the optimal policy initialization through integrating both directions of KL divergence.

5.2 Effectiveness analysis

To rigorously analyze the effectiveness of the proposed Bidirectional SAC algorithm, and specifically the Forward SAC component, two key questions must be addressed: (1) How accurately does the VDN-a network learn the marginal distribution? (2) Is the optimal projection policy $\pi_{\text{new-f}}$, derived by optimizing the forward KL divergence, demonstrably closer to the target Boltzmann distribution $q(\cdot|s_t)$ than the traditional updated policy $\pi_{\text{new-r}}$, obtained via gradient optimization of reverse KL divergence? To provide insight into these questions, we examine the training process of Bidirectional SAC within the Hopper environment. The Hopper environment’s action space is three-dimensional, which facilitates analysis and serves as a suitable testbed for validating our claims. We analyze data from two distinct updating steps during training. Figure 5 presents a comparison between the estimated marginal distribution $q_i(\cdot|s_t)$ and the ground truth marginal distribution $q_i^*(\cdot|s_t)$. The true marginal distribution is readily computed via multidimensional numerical integration of $q(\cdot|s_t)$. As depicted in the figure, while the estimated marginal distribution $q_i(\cdot|s_t)$ exhibits some deviation from the true distribution, it successfully captures the principal characteristics of the

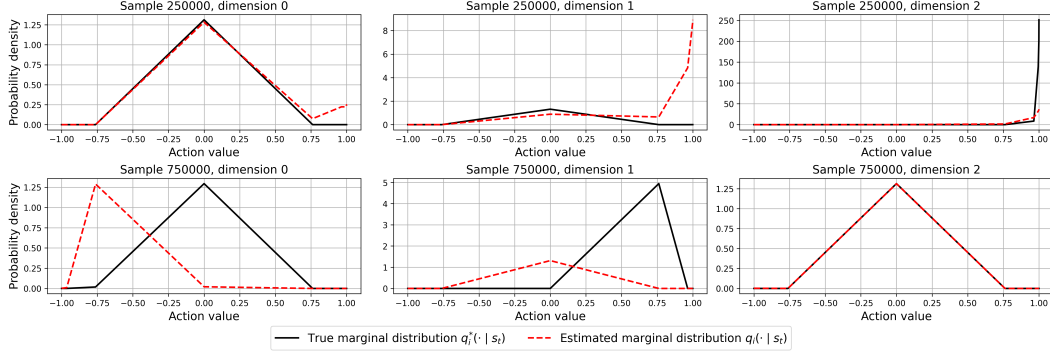


Figure 5: The comparison result in marginal distribution learned by VDN-a networks to the true distribution.

ground truth, particularly the mean and variance information critical for the updating mechanism in Bidirectional SAC. Addressing the second question, Figure 6 illustrates a comparison of the updated policy distributions from Forward SAC and standard SAC at the same training step. The figure clearly indicates that the updated policy distribution resulting from Forward SAC more closely resembles the target distribution $q(\cdot | s_t)$ than the policy updated using the standard SAC algorithm’s reverse KL approach, thereby answering the second question affirmatively. Further comparisons of policy distributions during the updating steps are provided in Appendix F.2.

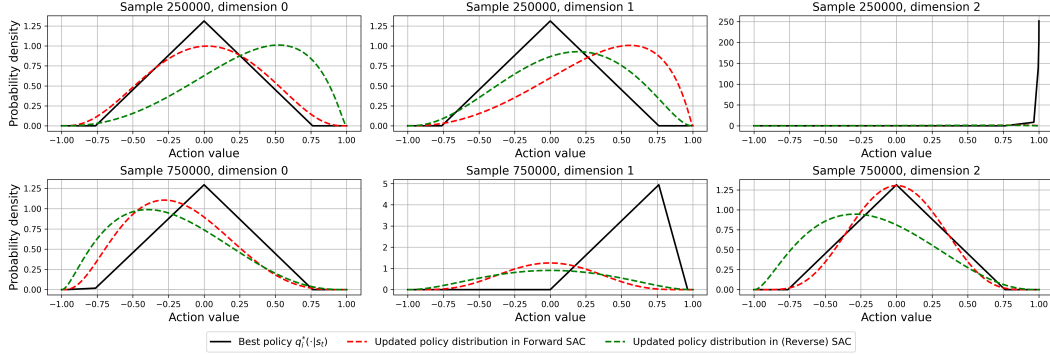


Figure 6: The comparison result for the updated policy in Forward SAC and standard SAC to the Boltzmann distribution $q(a_t | s_t)$.

6 Conclusion and future work

This paper addressed the optimization challenges of reverse KL divergence in the SAC algorithm. We demonstrated that employing forward KL divergence permits an explicit optimal policy projection, calculable via numerical integration and facilitated by our proposed VDN-a critic architecture. Building upon this insight, we introduced Bidirectional SAC, an algorithm that combines the direct policy computation inherent in forward KL with the policy improvement guarantees associated with reverse KL. Empirical results show that Bidirectional SAC significantly surpasses standard SAC and other baselines in both sample efficiency and asymptotic performance, achieving up to a 30% increase in episodic rewards.

Despite these advancements, we acknowledge that the optimal projection policy in the forward KL component is approximated using the VDN-a network, and the actor updates in Bidirectional SAC still rely on gradient descent due to neural network parameterization. While our extensive experiments validate the superior performance of Bidirectional SAC, further research could aim to bridge the gap between these practical approximations and the theoretically true optimal projection policy. Exploring methods for even more accurate policy projections and refined optimization techniques within this bidirectional framework presents a promising avenue for future investigation.

References

- Abbas Abdolmaleki, Bob Price, Nuno Lau, Luis Paulo Reis, and Gerhard Neumann. Deriving and improving cma-es with information geometric trust regions. In *Proceedings of the Genetic and Evolutionary Computation Conference*, pages 657–664, 2017.
- Abbas Abdolmaleki, Jost Tobias Springenberg, Yuval Tassa, Remi Munos, Nicolas Heess, and Martin Riedmiller. Maximum a posteriori policy optimisation. In *International Conference on Learning Representations*, 2018a.
- Abbas Abdolmaleki, Jost Tobias Springenberg, Yuval Tassa, Remi Munos, Nicolas Heess, and Martin Riedmiller. Maximum a posteriori policy optimisation. *arXiv preprint arXiv:1806.06920*, 2018b.
- Chayan Banerjee, Zhiyong Chen, and Nasimul Noman. Improved soft actor-critic: Mixing prioritized off-policy samples with on-policy experiences. *IEEE Transactions on Neural Networks and Learning Systems*, 35(3):3121–3129, 2022.
- Sumeet Batra, Bryon Tjanaka, Matthew Christopher Fontaine, Aleksei Petrenko, Stefanos Nikolaidis, and Gaurav S. Sukhatme. Proximal policy gradient arborescence for quality diversity reinforcement learning. In *International Conference on Learning Representations*, 2024.
- Erin Catto. Box2d: A 2d physics engine for games. URL: <http://www.box2d.org>, 2011.
- Alan Chan, Hugo Silva, Sungsu Lim, Tadashi Kozuno, A Rupam Mahmood, and Martha White. Greedification operators for policy optimization: Investigating forward and reverse kl divergences. *Journal of Machine Learning Research*, 23(253):1–79, 2022.
- Peter Dayan and Geoffrey E Hinton. Using expectation-maximization for reinforcement learning. *Neural Computation*, 9(2):271–278, 1997.
- Junior Costa de Jesus, Victor Augusto Kich, Alisson Henrique Kolling, Ricardo Bedin Grando, Marco Antonio de Souza Leite Cuadros, and Daniel Fernando Tello Gamarra. Soft actor-critic for navigation of mobile robots. *Journal of Intelligent & Robotic Systems*, 102(2):31, 2021.
- Jingliang Duan, Yang Guan, Shengbo Eben Li, Yangang Ren, Qi Sun, and Bo Cheng. Distributional soft actor-critic: Off-policy reinforcement learning for addressing value estimation errors. *IEEE transactions on Neural Networks and Learning Systems*, 33(11):6584–6598, 2021a.
- Jingliang Duan, Yang Guan, Shengbo Eben Li, Yangang Ren, Qi Sun, and Bo Cheng. Distributional soft actor-critic: Off-policy reinforcement learning for addressing value estimation errors. *IEEE Transactions on Neural Networks and Learning Systems*, 33(11):6584–6598, 2021b.
- Matthew Fellows, Anuj Mahajan, Tim GJ Rudner, and Shimon Whiteson. Virel: A variational inference framework for reinforcement learning. *Advances in Neural Information Processing Systems*, 32, 2019.
- Daniel Freeman, Erik Frey, Anton Raichuk, Sertan Girgin, Igor Mordatch, and Olivier Bachem. Brax - a differentiable physics engine for large scale rigid body simulation. In *Proceedings of the Neural Information Processing Systems Track on Datasets and Benchmarks*, 2021.
- Divyansh Garg, Shuvam Chakraborty, Chris Cundy, Jiaming Song, and Stefano Ermon. Iq-learn: Inverse soft-q learning for imitation. *Advances in Neural Information Processing Systems*, 34, 2021.
- Tuomas Haarnoja, Haoran Tang, Pieter Abbeel, and Sergey Levine. Reinforcement learning with deep energy-based policies. In *Proceedings of the 34th International Conference on Machine Learning*, pages 1352–1361, 2017.
- Tuomas Haarnoja, Aurick Zhou, Pieter Abbeel, and Sergey Levine. Soft actor-critic: Off-policy maximum entropy deep reinforcement learning with a stochastic actor. In *Proceedings of the 35th International Conference on Machine Learning*, pages 1861–1870, 2018a.
- Tuomas Haarnoja, Aurick Zhou, Kristian Hartikainen, George Tucker, Sehoon Ha, Jie Tan, Vikash Kumar, Henry Zhu, Abhishek Gupta, Pieter Abbeel, et al. Soft actor-critic algorithms and applications. *arXiv preprint arXiv:1812.05905*, 2018b.

- Aicke Hinrichs, Erich Novak, Mario Ullrich, and H Woźniakowski. The curse of dimensionality for numerical integration of smooth functions. *Mathematics of Computation*, 83(290):2853–2863, 2014.
- Yifan Hu, Junjie Fu, and Guanghui Wen. Graph soft actor–critic reinforcement learning for large-scale distributed multirobot coordination. *IEEE Transactions on Neural Networks and Learning Systems*, 36(1):665–676, 2025.
- Shengyi Huang, Rousslan Fernand Julien Dossa, Chang Ye, Jeff Braga, Dipam Chakraborty, Kinal Mehta, and JoˆGo GM Araˆsjo. Cleanrl: High-quality single-file implementations of deep reinforcement learning algorithms. *Journal of Machine Learning Research*, 23(274):1–18, 2022.
- Dongyoung Kim, Jinwoo Shin, Pieter Abbeel, and Younggyo Seo. Accelerating reinforcement learning with value-conditional state entropy exploration. *Advances in Neural Information Processing Systems*, 36, 2024.
- Taisuke Kobayashi. Optimistic reinforcement learning by forward kullback–leibler divergence optimization. *Neural Networks*, 152:169–180, 2022.
- Aviral Kumar, Aurick Zhou, George Tucker, and Sergey Levine. Conservative q-learning for offline reinforcement learning. *Advances in Neural Information Processing Systems*, 33, 2020.
- TP Lillicrap. Continuous control with deep reinforcement learning. *arXiv preprint arXiv:1509.02971*, 2015.
- Zuxin Liu, Zhepeng Cen, Vladislav Isenbaev, Wei Liu, Steven Wu, Bo Li, and Ding Zhao. Constrained variational policy optimization for safe reinforcement learning. In *International Conference on Machine Learning*, pages 13644–13668, 2022.
- William Marshall McKeeman. Algorithm 145: Adaptive numerical integration by simpson’s rule. *Communications of the ACM*, 5(12):604, 1962.
- Jincheng Mei, Chenjun Xiao, Ruitong Huang, Dale Schuurmans, and Martin Mller. On principled entropy exploration in policy optimization. In *Proceedings of the 28th International Joint Conference on Artificial Intelligence*, pages 3130–3136, 2019.
- Alberto Maria Metelli, Matteo Papini, Nico Montali, and Marcello Restelli. Importance sampling techniques for policy optimization. *Journal of Machine Learning Research*, 21(141):1–75, 2020.
- Volodymyr Mnih, Koray Kavukcuoglu, David Silver, Andrei A Rusu, Joel Veness, Marc G Bellemare, Alex Graves, Martin Riedmiller, Andreas K Fidjeland, Georg Ostrovski, et al. Human-level control through deep reinforcement learning. *Nature*, 518(7540):529–533, 2015.
- Volodymyr Mnih, Adria Puigdomenech Badia, Mehdi Mirza, Alex Graves, Timothy Lillicrap, Tim Harley, David Silver, and Koray Kavukcuoglu. Asynchronous methods for deep reinforcement learning. In *Proceedings of The 33rd International Conference on Machine Learning*, pages 1928–1937, 2016.
- Ofir Nachum, Mohammad Norouzi, and Dale Schuurmans. Improving policy gradient by exploring under-appreciated rewards. *arXiv preprint arXiv:1611.09321*, 2016.
- Antonin Raffin, Ashley Hill, Adam Gleave, Anssi Kanervisto, Maximilian Ernestus, and Noah Dormann. Stable-baselines3: Reliable reinforcement learning implementations. *Journal of Machine Learning Research*, 22(268):1–8, 2021.
- John Schulman, Sergey Levine, Pieter Abbeel, Michael Jordan, and Philipp Moritz. Trust region policy optimization. In *Proceedings of the 32nd International Conference on Machine Learning*, pages 1889–1897, 2015.
- John Schulman, Filip Wolski, Prafulla Dhariwal, Alec Radford, and Oleg Klimov. Proximal policy optimization algorithms. *arXiv preprint arXiv:1707.06347*, 2017.
- Alexander Shapiro. Monte carlo sampling methods. *Handbooks in Operations Research and Management Science*, 10:353–425, 2003.

- H Francis Song, Abbas Abdolmaleki, Jost Tobias Springenberg, Aidan Clark, Hubert Soyer, Jack W Rae, Seb Noury, Arun Ahuja, Siqi Liu, Dhruva Tirumala, et al. V-mpo: On-policy maximum a posteriori policy optimization for discrete and continuous control. In *International Conference on Learning Representations*, 2020.
- Peter Sunehag, Guy Lever, Audrunas Gruslys, Wojciech Marian Czarnecki, Vinicius Zambaldi, Max Jaderberg, Marc Lanctot, Nicolas Sonnerat, Joel Z Leibo, Karl Tuyls, et al. Value-decomposition networks for cooperative multi-agent learning. *arXiv preprint arXiv:1706.05296*, 2017.
- Richard S. Sutton and Andrew G. Barto. *Reinforcement Learning: An Introduction*. A Bradford Book, 2018.
- Emanuel Todorov, Tom Erez, and Yuval Tassa. Mujoco: A physics engine for model-based control. In *2012 IEEE/RSJ International Conference on Intelligent Robots and Systems*, pages 5026–5033, 2012.
- Marc Toussaint and Amos Storkey. Probabilistic inference for solving discrete and continuous state markov decision processes. In *Proceedings of the 23rd international conference on Machine learning*, pages 945–952, 2006.
- Yi Wang, Hui Tang, Lichao Huang, Lulu Pan, Lixiang Yang, Huanming Yang, Feng Mu, and Meng Yang. Self-play reinforcement learning guides protein engineering. *Nature Machine Intelligence*, 5(8):845–860, 2023.
- Yuhuai Wu, Elman Mansimov, Roger B Grosse, Shun Liao, and Jimmy Ba. Scalable trust-region method for deep reinforcement learning using kronecker-factored approximation. *Advances in Neural Information Processing Systems*, 30, 2017.
- Jiachen Yang, Jiankun Peng, Quanwei Zhang, Weiqi Chen, and Chunye Ma. Monocular vision approach for soft actor-critic based car-following strategy in adaptive cruise control. *Expert Systems with Applications*, page 125999, 2024.
- Qisong Yang, Thiago D Simão, Simon H Tindemans, and Matthijs TJ Spaan. Wcsac: Worst-case soft actor critic for safety-constrained reinforcement learning. In *Proceedings of the AAAI Conference on Artificial Intelligence*, pages 10639–10646, 2021.
- Brian D Ziebart, Andrew L Maas, J Andrew Bagnell, Anind K Dey, et al. Maximum entropy inverse reinforcement learning. In *Proceedings of the AAAI Conference on Artificial Intelligence*, pages 1433–1438, 2008.
- Hanna Ziesche and Leonel Roza. Wasserstein gradient flows for optimizing gaussian mixture policies. *Advances in Neural Information Processing Systems*, 36, 2024.

A KL divergence derivation

We need to compute the partial derivatives of the objective function

$$D_{\text{KL}}(q(\cdot | s_t) || \pi'(a | s_t))$$

with respect to $f_{\phi}^i(s_t)$ and Σ_{ϕ}^i . Given that $\pi'(a | s_t) = \prod_i \pi'_i(a^i | s_t)$, where each $\pi'_i(a^i | s_t) = \mathcal{N}(a^i; f_{\phi}^i(s_t), \Sigma_{\phi}^i)$, we will derive the necessary expressions by considering the marginal normal distributions’ mean and variance.

A.1 Expanding the KL divergence expression

According to the definition of KL divergence:

$$D_{\text{KL}}(q(\cdot | s_t) || \pi'(a | s_t)) = \int_{\mathcal{A}} q(a | s_t) \log q(a | s_t) - q(a | s_t) \log \pi'(a | s_t) da.$$

Since $\pi'(a | s_t)$ is a product of individual components:

$$\pi'(a | s_t) = \prod_i \pi'_i(a^i | s_t),$$

We have:

$$\log \pi'(a \mid s_t) = \sum_i \log \pi'_i(a^i \mid s_t).$$

Thus, the KL divergence becomes:

$$\begin{aligned} D_{\text{KL}}(q(\cdot \mid s_t) \parallel \pi'(a \mid s_t)) &= \int_{\mathcal{A}} q(a \mid s_t) \log q(a \mid s_t) da \\ &+ \sum_i \frac{1}{2} \log(2\pi\Sigma_\phi^i) \int_{\mathcal{A}} q(a \mid s_t) da - \sum_i \frac{1}{2\Sigma_\phi^i} \int_{\mathcal{A}} q_i(a^i \mid s_t)(a^i - f_\phi^i(s_t))^2 da^i. \end{aligned} \quad (8)$$

Since $\int_{\mathcal{A}} q(a \mid s_t) da = 1$, the second term simplifies to:

$$\sum_i \frac{1}{2} \log(2\pi\Sigma_\phi^i).$$

The third term corresponds to the variance term of $q_i(a^i \mid s_t)$.

A.2 Partial derivatives with respect to $f_\phi^i(s_t)$ and Σ_ϕ^i

A.2.1 Derivative with respect to $f_\phi^i(s_t)$

We need to compute the terms involving $f_\phi^i(s_t)$. The relevant term is:

$$\sum_i \frac{1}{2\Sigma_\phi^i} \int_{\mathcal{A}} q_i(a^i \mid s_t)(a^i - f_\phi^i(s_t))^2 da^i.$$

Taking the derivative with respect to $f_\phi^i(s_t)$, we get:

$$\frac{\partial}{\partial f_\phi^i(s_t)} \left(\frac{1}{2\Sigma_\phi^i} \int_{\mathcal{A}_i} q_i(a^i \mid s_t)(a^i - f_\phi^i(s_t))^2 da^i \right) = \frac{1}{\Sigma_\phi^i} \int_{\mathcal{A}_i} q_i(a^i \mid s_t)(a^i - f_\phi^i(s_t)) da^i.$$

This is the derivative of the mean $f_\phi^i(s_t)$ of the marginal normal distribution, which corresponds to the first moment (i.e., the mean) of $q_i(a^i \mid s_t)$.

A.2.2 Derivative with respect to Σ_ϕ^i

To compute the derivative with respect to Σ_ϕ^i , we differentiate each term:

$$\frac{\partial}{\partial \Sigma_\phi^i} \left(\frac{1}{2} \log(2\pi\Sigma_\phi^i) \right) = \frac{1}{2\Sigma_\phi^i}.$$

For the second term:

$$\frac{\partial}{\partial \Sigma_\phi^i} \left(\frac{1}{2\Sigma_\phi^i} \int_{\mathcal{A}_i} q_i(a^i \mid s_t)(a^i - f_\phi^i(s_t))^2 da^i \right) = -\frac{1}{2(\Sigma_\phi^i)^2} \int_{\mathcal{A}_i} q_i(a^i \mid s_t)(a^i - f_\phi^i(s_t))^2 da^i.$$

Thus, the partial derivative with respect to Σ_ϕ^i is:

$$\frac{\partial D_{\text{KL}}}{\partial \Sigma_\phi^i} = \frac{1}{2\Sigma_\phi^i} - \frac{1}{2(\Sigma_\phi^i)^2} \int_{\mathcal{A}_i} q_i(a^i \mid s_t)(a^i - f_\phi^i(s_t))^2 da^i.$$

B Squashing function

In case the action space is typically bounded by using an invertible squashing function, the optimal policy projection calculation should be adjusted for this transformation.

Recalling the definition of KL divergence:

$$D_{\text{KL}}(q(\cdot \mid s_t) \parallel \pi'(a \mid s_t)) = \int_{\mathcal{A}} q(a \mid s_t) \log q(a \mid s_t) - q(a \mid s_t) \log \pi'(a \mid s_t) da.$$

If we use a transformation $a = h(x)$, where $h(\cdot)$ is the squashing function to transform the original action value x to fit the action space in a specific environment. Without loss of generality, we assume $h(\cdot)$ is consistent in each dimension of the action, which means that $(a^1, a^2, \dots, a^N) = (h(x^1), h(x^2), \dots, h(x^N))$. Therefore, the probability density function is given by:

$$\pi'(a^i | s_t) = \pi'(x^i | s_t) \left| \frac{dx^i}{dh(x^i)} \right| = \frac{1}{\sqrt{2\pi\Sigma_\phi^i}} \exp\left(-\frac{(x^i - f_\phi^i(s_t))^2}{2\Sigma_\phi^i}\right) \left| \frac{1}{h'(x^i)} \right|$$

Substituting $\pi(y)$ into the KL divergence, we can obtain the partial derivative with respect to μ as:

$$\begin{aligned} \frac{\partial D_{\text{KL}}(q(\cdot | s_t) || \pi'(a | s_t))}{\partial f_\phi^i(s_t)} &= - \int_{\mathcal{A}} q(a | s_t) \frac{\partial}{\partial f_\phi^i(s_t)} \log(\pi'(h^{-1}(a) | s_t)) da \\ &= - \int_{-\infty}^{\infty} q(h(x^i) | s_t) \frac{\partial}{\partial f_\phi^i(s_t)} \log(\pi'(x^i | s_t)) h'(x^i) dx^i \\ &= \frac{1}{\Sigma_\phi^i} \int_{\mathcal{A}} q(h(x^i) | s_t) (x^i - f_\phi^i(s_t)) h'(x^i) dx^i \end{aligned}$$

Therefore, it is easily derived that the optimal mean value $f_\phi^i(s_t)$ is

$$f_\phi^i(s_t) = \int_{-\infty}^{\infty} q_i(h(x^i) | s_t) \cdot x^i \cdot h'(x^i) dx^i.$$

Similarly, the partial derivative with respect to Σ_ϕ^i is:

$$\frac{\partial D_{\text{KL}}(q(\cdot | s_t) || \pi'(a | s_t))}{\partial \Sigma_\phi^i} = \frac{1}{2\Sigma_\phi^i} - \frac{1}{2(\Sigma_\phi^i)^2} \int_{-\infty}^{\infty} q_i(h(x^i) | s_t) (x^i - f_\phi^i(s_t))^2 dx^i.$$

Therefore, the optimal variance

$$\Sigma_\phi^i = \int_{-\infty}^{\infty} q_i(h(x^i) | s_t) (x^i - f_\phi^i(s_t))^2 dx^i$$

By substituting the squashing function $h(\cdot)$ with $\tanh(\cdot)$, the ultimate optimal projection policy in Equation (12) is easily attained.

C The VDN-a network

C.1 The introduction to the VDN network

To compute the optimal policy parameters $f^i(s_t)^*$ and Σ^{i*} (mean and variance of the target Boltzmann distribution's marginals), various methods could be considered. Importance sampling [Shapiro, 2003], common in policy optimization [Metelli et al., 2020] and regularized reinforcement learning [Nachum et al., 2016, Mei et al., 2019], faces challenges in identifying a suitable proposal distribution that closely approximates the target [Nachum et al., 2016]. Numerical integration offers an alternative, but standard multidimensional integration suffers from the curse of dimensionality [Hinrichs et al., 2014], making it computationally prohibitive for high-dimensional action spaces. Even if $f^i(s_t)^*$ and Σ^{i*} are computed per dimension, obtaining the true marginal distribution $q_i(\cdot | s_t)$ of the full Boltzmann distribution $q(\cdot | s_t)$ remains difficult due to the complex dependencies between action dimensions.

To address these challenges, we propose the VDN-a network. This architecture is inspired by Value Decomposition Networks (VDN) [Sunehag et al., 2017], a significant advancement in Multi-Agent Reinforcement Learning (MARL) for cooperative systems with decentralized execution. The core idea of VDN, illustrated in Figure 7, is to decompose a global value function $Q_{total}(s, a)$ into a sum of individual agent-specific value functions $Q_i(s_i, a_i)$:

$$Q_{total}(s, a) = \sum_{i=1}^N Q_i(s_i, a_i) \quad (9)$$

where s_i and a_i are the local observation and action for agent i . This additivity allows each agent to make decisions based on its local value function, while the system is trained centrally. VDNs support scalability and are effective in cooperative scenarios where the team’s objective can be approximated as a sum of individual contributions, offering benefits like reduced complexity and improved credit assignment.

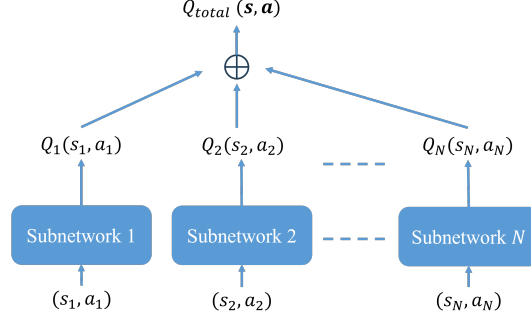


Figure 7: Framework of the original Value Decomposition Network (VDN) for MARL.

The additive structure of VDN has proven effective in MARL and provides a foundation for more sophisticated value decomposition methods. In our single-agent context, we adapt this principle in the VDN-a network (detailed in Section 3.3 of the main paper and Figure 2) not to decompose by agent, but to structure the Q-function $Q(s_t, a_t)$ such that components primarily related to individual action dimensions a_t^i can be learned by subnetworks $Q_i(s_t, a_t^i)$, with an auxiliary network $U(s_t, a_t)$ capturing interactions. This facilitates the estimation of terms related to the marginals of the Boltzmann distribution, as theoretically justified below.

C.2 Theoretical foundation for VDN-a network using copula theory

This section provides a theoretical framework, grounded in Copula theory, to explain how the VDN-a network architecture facilitates the learning of components essential for recovering the true marginal distributions of the Boltzmann target distribution $q(a|s_t)$. This capability is crucial for the Forward SAC component of our Bidirectional SAC algorithm, which relies on the mean and variance of these marginals.

C.2.1 Sklar’s theorem and preliminary definitions

Let $a = (a_1, a_2, \dots, a_n)$ be an n -dimensional action vector in $\mathcal{A} \subseteq \mathbb{R}^n$ for a given state $s_t \in \mathcal{S}$.

- $Q^{\pi_{\text{old}}}(s_t, a)$: The soft Q-function from the previous policy π_{old} .
- $Q_{\text{Boltz}}(a; s_t) \equiv \frac{1}{\alpha} Q^{\pi_{\text{old}}}(s_t, a)$: The potential function for the Boltzmann distribution at state s_t , where α is the temperature parameter. For conciseness, $Q_{\text{Boltz}}(a)$ is used when s_t is implicit.
- $Z(s_t) = \int_{\mathcal{A}} \exp(Q_{\text{Boltz}}(a'; s_t)) da'$: The partition function for $q(a|s_t)$.
- $q(a|s_t) = \frac{\exp(Q_{\text{Boltz}}(a; s_t))}{Z(s_t)}$: The target Boltzmann joint PDF over actions.
- $M^{(j)}(a_j; s_t) \equiv \int_{\mathcal{A}_{-j}} \exp(Q_{\text{Boltz}}(a_j, a'_{-j}; s_t)) da'_{-j}$: The marginalization of $\exp(Q_{\text{Boltz}}(a; s_t))$ over action dimensions except a_j . The term $\ln(M^{(j)}(a_j; s_t))$ is central to what VDN-a subnetworks aim to capture.
- $q_j(a_j|s_t) = \frac{M^{(j)}(a_j; s_t)}{Z(s_t)}$: The j -th true marginal PDF of $q(a|s_t)$.
- $F_j(a_j|s_t) = \int_{-\infty}^{a_j} q_j(t_j|s_t) dt_j$: The j -th true marginal CDF.
- $c(u_1, \dots, u_n; s_t)$: The unique copula density function associated with $q(a|s_t)$.
- $\mathcal{L}_c(a; s_t) \equiv \ln(c(F_1(a_1|s_t), \dots, F_n(a_n|s_t); s_t))$: The log-copula density term.

Sklar's Theorem states that any joint PDF $q(a|s_t)$ can be expressed via its marginal CDFs $F_j(a_j|s_t)$ and a unique copula density $c(\cdot; s_t)$. In terms of densities:

$$q(a|s_t) = c(F_1(a_1|s_t), \dots, F_n(a_n|s_t); s_t) \prod_{j=1}^n q_j(a_j|s_t) \quad (10)$$

C.2.2 Derivation of the structural expression for $Q_{\text{Boltz}}(a; s_t)$

We decompose $Q_{\text{Boltz}}(a; s_t)$ using Eq. (10). Given $q(a|s_t) = \exp(Q_{\text{Boltz}}(a; s_t))/Z(s_t)$, equating this with Eq. (10) and taking logarithms yields:

$$Q_{\text{Boltz}}(a; s_t) - \ln(Z(s_t)) = \ln(c(F_1(a_1|s_t), \dots, F_n(a_n|s_t); s_t)) + \sum_{j=1}^n \ln(q_j(a_j|s_t))$$

Using $\mathcal{L}_c(a; s_t) = \ln(c(\dots))$ and substituting $q_j(a_j|s_t) = M^{(j)}(a_j; s_t)/Z(s_t)$:

$$Q_{\text{Boltz}}(a; s_t) = \ln(Z(s_t)) + \sum_{j=1}^n \left(\ln(M^{(j)}(a_j; s_t)) - \ln(Z(s_t)) \right) + \mathcal{L}_c(a; s_t)$$

This simplifies to:

$$Q_{\text{Boltz}}(a; s_t) = (1 - n) \ln(Z(s_t)) + \sum_{j=1}^n \ln(M^{(j)}(a_j; s_t)) + \mathcal{L}_c(a; s_t) \quad (11)$$

This exact decomposition reveals $Q_{\text{Boltz}}(a; s_t)$ as a sum of a state-dependent constant, terms $\ln(M^{(j)}(a_j; s_t))$ (each depending only on a_j and s_t), and an interaction term $\mathcal{L}_c(a; s_t)$ capturing multivariate dependencies.

C.2.3 VDN-a network and its connection to the Copula decomposition

The VDN-a network approximates $Q^{\pi_{\text{old}}}(s_t, a)$ as $Q^{\text{VDN-a}}(s_t, a) = \sum_{j=1}^n Q_j^{\text{sub}}(s_t, a_j) + U^{\text{aux}}(s_t, a)$. The corresponding learned potential function is $Q_{\text{Boltz}}^{\text{VDN-a}}(a; s_t) = \frac{1}{\alpha} Q^{\text{VDN-a}}(s_t, a)$, so:

$$Q_{\text{Boltz}}^{\text{VDN-a}}(a; s_t) = \sum_{j=1}^n \underbrace{\left(\frac{1}{\alpha} Q_j^{\text{sub}}(s_t, a_j) \right)}_{\equiv \hat{Q}_j^*(a_j; s_t)} + \underbrace{\left(\frac{1}{\alpha} U^{\text{aux}}(s_t, a) \right)}_{\equiv \hat{U}^*(a; s_t)}$$

If $Q_{\text{Boltz}}^{\text{VDN-a}}(a; s_t) \approx Q_{\text{Boltz}}(a; s_t)$, the VDN-a structure aims for:

- Each $\hat{Q}_j^*(a_j; s_t)$ to primarily learn $\ln(M^{(j)}(a_j; s_t))$ plus absorbable state-dependent constants $k_j(s_t)$. Thus, $\exp(\hat{Q}_j^*(a_j; s_t)) \propto M^{(j)}(a_j; s_t)$. Crucially, $Q_j^{\text{sub}}(s_t, a_j)$ is not an isolated "marginal Q-value" but learns the component of $Q^{\pi_{\text{old}}}$ corresponding to $\ln(M^{(j)})$, given U^{aux} handles interactions.
- $\hat{U}^*(a; s_t)$ to primarily learn the log-copula density $\mathcal{L}_c(a; s_t)$ and remaining constants from Eq. (11).

C.2.4 Recovery of true marginal distributions

The estimated marginal distributions are $\hat{q}_j(a_j|s_t) = \frac{\exp(\hat{Q}_j^*(a_j; s_t))}{\int_{\mathcal{A}_j} \exp(\hat{Q}_j^*(a'_j; s_t)) da'_j}$. If $\exp(\hat{Q}_j^*(a_j; s_t)) = K_j(s_t) M^{(j)}(a_j; s_t)$ for some $K_j(s_t) > 0$, the denominator becomes $K_j(s_t) \int_{\mathcal{A}_j} M^{(j)}(a'_j; s_t) da'_j$. Since $\int_{\mathcal{A}_j} M^{(j)}(a'_j; s_t) da'_j = Z(s_t)$, then:

$$\hat{q}_j(a_j|s_t) = \frac{K_j(s_t) M^{(j)}(a_j; s_t)}{K_j(s_t) Z(s_t)} = \frac{M^{(j)}(a_j; s_t)}{Z(s_t)} = q_j(a_j|s_t)$$

Thus, if each $\frac{1}{\alpha} Q_j^{\text{sub}}(s_t, a_j)$ effectively learns $\ln(M^{(j)}(a_j; s_t))$ (up to an additive constant, implying $\exp(\frac{1}{\alpha} Q_j^{\text{sub}})$ captures $M^{(j)}$ up to a multiplicative constant), and U^{aux} isolates dependencies, then this procedure recovers the true marginal PDFs.

Condition of a "sufficiently learned" auxiliary network or independence: The main paper's assertion that "if the auxiliary network is sufficiently learned or each dimension of the action is independent, the learned $q_i(a_t^i | s_t)$ is actually the true marginal distribution of the $q(\cdot | s_t)$ " is supported:

- **Sufficiently learned U^{aux} :** If U^{aux} correctly models $\mathcal{L}_c(a; s_t)$ and other non-separable terms, Q_j^{sub} can accurately represent components related to $M^{(j)}(a_j; s_t)$, leading to correct $q_j(a_j | s_t)$ recovery.
- **Independence:** If action dimensions are independent, $c(\dots; s_t) = 1$, so $\mathcal{L}_c(a; s_t) = 0$. Then $Q_{\text{Boltz}}(a; s_t) = (1 - n) \ln(Z(s_t)) + \sum_{j=1}^n \ln(M^{(j)}(a_j; s_t))$. If $\hat{U}^*(a; s_t)$ learns the resulting constant term, each $\hat{Q}_j^*(a_j; s_t)$ more directly approximates $\ln(M^{(j)}(a_j; s_t))$, making marginal recovery robust.

Figures 8 and 9 illustrate VDN-a's empirical performance in approximating marginal distribution components. Figure 8 shows effective learning for unimodal target marginal components, while Figure 9 indicates that performance can be challenged by more complex, e.g., bimodal, marginal structures. This challenge may arise from the increased difficulty for U^{aux} to perfectly model the intricate dependencies (the copula term \mathcal{L}_c) needed to cleanly isolate the $\ln(M^{(j)})$ terms in such cases. However, as observed in typical RL training states (e.g., Figure 5 in the main text), target marginals are often adequately approximated as unimodal. Critically, the first two moments (mean and variance)—primarily required by our Forward SAC component—are often still well-captured by VDN-a estimations even with these complexities. Consequently, the VDN-a network provides a practically effective approach for approximating the necessary marginal properties within our Bidirectional SAC framework.

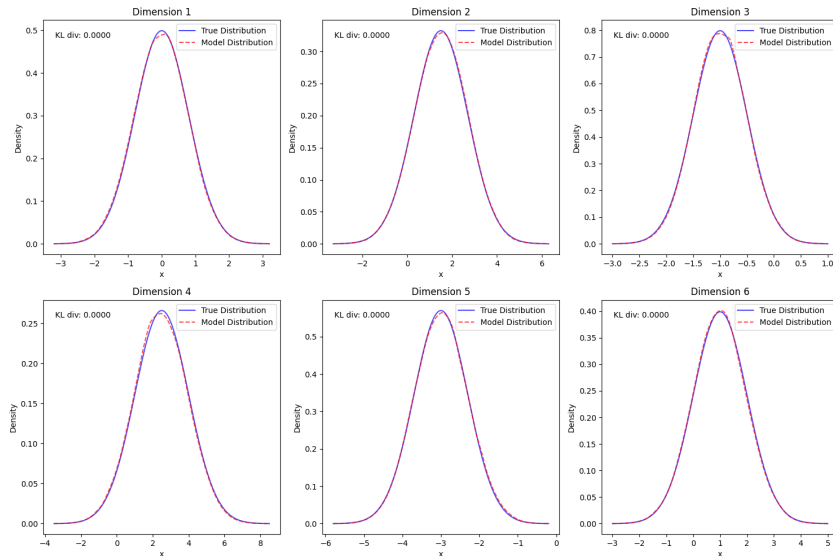


Figure 8: VDN-a performance in approximating components related to a unimodal marginal distribution. (Assumed: Solid lines might be true components/PDF, dashed are VDN-a estimates - clarify in actual caption based on what is plotted).

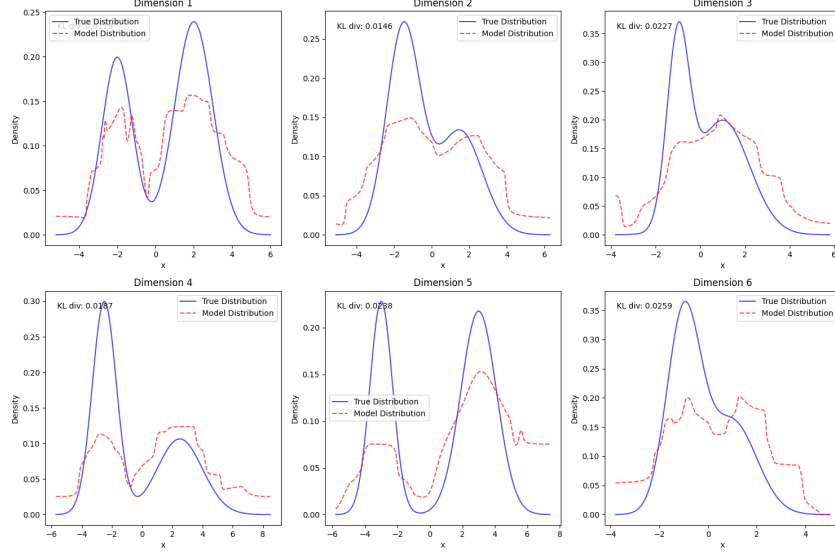


Figure 9: VDN-a performance in approximating components related to a bimodal marginal distribution. (Assumed: Solid lines might be true components/PDF, dashed are VDN-a estimates - clarify in actual caption).

D More details of the Forward SAC algorithm

D.1 The implementation details of the Forward SAC algorithm

The Forward SAC can be obtained from SAC by changing both the learning of the critic and actor in the following steps: for the critic, it uses the VDN-a network to serve as the Q-function, with the updating rule remaining the same as SAC; for the actor, Forward SAC uses the forward KL divergence and the explicit form of optimal projection policy, while the actor network learns directly from the mean and variance of the Boltzmann distribution $q_i(\cdot | s_t)$.

In case the action space is typically bounded by using an invertible squashing function, such as $\tanh(\cdot)$ [Haarnoja et al., 2018b, Duan et al., 2021a], to squash the action samples from the Gaussian policy, the parameters for ultimate optimal projection policy is adapted as:

$$\begin{aligned}
 f^i(s_t)^* &= \int_{-b}^b q_i(\tanh(x) | s_t) \cdot x \cdot \tanh'(x) dx, \\
 \Sigma^{i*} &= \int_{-b}^b q_i(\tanh(x) | s_t) \cdot (x - \mu)^2 \cdot \tanh'(x) dx, \\
 q_i(\cdot | s_t) &= \frac{\exp\left(\frac{1}{\alpha} Q_i(s_t, \cdot)\right)}{\int_{-b}^b \exp\left(\frac{1}{\alpha} Q_i(s_t, \tanh(x))\right) \tanh'(x) dx}
 \end{aligned} \tag{12}$$

where $\tanh'(x) = (1 - \tanh^2(x))$ is the derivative of $\tanh(x)$, and b is a hyperparameter for the integration bound. The detailed derivation is described in Appendix B. The numerical integration methods are adapted for the calculation of the optimal projection policy in Equation (12). We employ the widely recognized Simpson's integration method [McKeeman, 1962]. We denote the Simpson's integration as $\mathcal{S}_a^b[\cdot]$, which is renowned for its computational efficiency and high accuracy. For a given interval $[a, b]$, the definite integral of a function $g(x)$ is approximated by Simpson's rule as follows:

$$\int_a^b g(x) dx \approx \mathcal{S}_a^b[g(x)] = \frac{h}{3} \left[g(x_0) + 4 \sum_{\substack{i=1 \\ i \text{ odd}}}^{I-1} g(x^i) + 2 \sum_{\substack{i=2 \\ i \text{ even}}}^{I-2} g(x^i) + g(x^I) \right], \tag{13}$$

where the interval $[a, b]$ is partitioned into I equally spaced subintervals of width $h = \frac{b-a}{I}$. The points $x_0 = a$ and $x^I = b$ denote the endpoints of the interval. The summations $\sum_{\text{odd}} g(x^i)$ and

$\sum_{\text{even}} g(x^i)$ represent the aggregate of function evaluations at interior points with odd and even indices, respectively.

Denoting the Simpson integration of the optimal projection policy as $\hat{f}^i(s_t)$ and $\hat{\Sigma}^i$, the Forward SAC algorithm can be implemented through two ways:

- (1) Only use the critic. The mean and variance of the optimal projection policy $\pi_{\text{new-f}}$ are calculated when interacting with the environment. This method ensures each iteration, the optimal projection policy is used.
- (2) Use both the critic and actor. The actor network is updated through MSE loss, which is stable and efficient, but this actor interacting with the environment is not the exactly optimal projection policy (which is similar to the implementation of the Bidirectional SAC algorithm).

Algorithm 2 Forward SAC algorithm (only critic)

Hyperparameters: Total number of training steps \mathcal{L} , number of time steps \mathcal{T} each update epoch, mini-batch size \mathcal{M} , the update epoch \mathcal{J} of neural networks each training, and the learning rate β .

- 1: Initialize the critic network Q_θ and replay buffer \mathcal{B} .
 - 2: Start with the initial state s_0
 - 3: **for** $l = 1, \dots, \mathcal{L}$ **do**
 - 4: **for** $t = 1, \dots, \mathcal{T}$ **do**
 - 5: Calculate the mean $f^i(s_t)^*$ and variance Σ^{i*} in Equation (12) through Simpson's rule in (13).
 - 6: Establish the optimal projection policy $\pi_{\text{new-f}}$ through $f^i(s_t)^*$ and Σ^{i*} .
 - 7: Sample actions from policy $\pi_{\text{new-f}}$, collect and store the transition (s_t, a_t, r_t, s_{t+1}) in replay buffer \mathcal{B} .
 - 8: **for** $j = 1, \dots, \mathcal{J}$ **do**
 - 9: Sample mini-batch $\{(s_i, a^i, r_i, s_{i+1}) \mid i = 1, \dots, \mathcal{M}\}$ from \mathcal{B} .
 - 10: Update the critic network Q_θ by $\theta \leftarrow \theta - \beta \nabla_\theta J_Q(\theta)$ in (2)
 - 11: **end for**
 - 12: **end for**
 - 13: **end for**
-

For (1), the algorithm is detailed in Algorithm 2. For (2), the actor is updated by the gradient of the MSE loss function $\nabla_\phi \text{MSE}(\pi_\phi)$:

$$\begin{aligned} & \nabla \sum_{i=1}^I \left[\left(\hat{f}^i(s_t) - f_\phi^i(s_t) \right)^2 + \left(\hat{\Sigma}^i - \Sigma_\phi^i \right)^2 \right] = \\ & 2 \sum_{i=1}^I \left[\left(\hat{f}^i(s_t) - f_\phi^i(s_t) \right) \nabla_\phi f_\phi^i(s_t) + \left(\hat{\Sigma}^i - \Sigma_\phi^i \right) \nabla_\phi \Sigma_\phi^i \right]. \end{aligned}$$

Then we show the algorithm of Forward SAC implemented as (2) in Algorithm 3. Two soft Q-function networks and their corresponding target networks are adopted in this paper, similar to the SAC algorithm. The target network is updated smoothly by soft updates, where a hyperparameter τ is used to control the updating speed.

D.2 The relation between Forward SAC and variational policy optimization

Variational policy optimization primarily relies on the EM method to iteratively update both the variational distribution and the policy. In the E-step [Abdolmaleki et al., 2018a], the variational distribution $v(a_t \mid s_t)$ is learned iteratively, given by

$$v(a_t \mid s_t) = \frac{\pi_\phi(a_t \mid s) \exp\left(\frac{1}{\alpha} Q_\theta(s, a_t)\right)}{\int_{\mathcal{A}} \pi_\phi(a \mid s) \exp\left(\frac{1}{\alpha} Q_\theta(s, a)\right) da}. \quad (14)$$

This is similar to the Boltzmann distribution $q(a_t \mid s_t)$. To update the policy, the M-step optimizes the ELBO with respect to ϕ :

$$\mathcal{J}(v, \phi) = \log p(\phi) + Q^v(s_t, \cdot) - \mathbb{E}_{\tau \sim v} \left[\sum_{t=0}^{\infty} (\alpha D_{\text{KL}}(v(\cdot \mid s_t) \parallel \pi_\phi(\cdot \mid s_t))) \right], \quad (15)$$

Algorithm 3 Forward SAC algorithm (use an actor)

Hyperparameters: Total number of training steps \mathcal{L} , mini-batch size \mathcal{M} , the update epoch \mathcal{T} of neural networks each training, and the learning rate β

- 1: Initialize the critic network Q_θ , actor network π_ϕ and replay buffer \mathcal{B} .
 - 2: Start with the initial state s_0
 - 3: **for** $l = 1, \dots, \mathcal{L}$ **do**
 - 4: Using policy π_ϕ , collect and store transitions (s_t, a_t, r_t, s_{t+1}) in replay buffer \mathcal{B} .
 - 5: **for** $j = 1, \dots, \mathcal{T}$ **do**
 - 6: Sample mini-batch $\{(s_i, a^i, r_i, s_{i+1}) \mid i = 1, \dots, \mathcal{M}\}$ from \mathcal{B} .
 - 7: Update the critic network Q_θ by $\theta \leftarrow \theta - \beta \nabla_\theta J_Q(\theta)$ in (2)
 - 8: Update the actor parameters with $\phi \leftarrow \phi - \eta \nabla_\phi MSE(\pi_\phi)$.
 - 9: **end for**
 - 10: **end for**
-

where $p(\phi)$ is the prior distribution, and $v(\cdot \mid s_t)$ is the variational distribution. If the prior distribution is set to the identity distribution, the optimization of the ELBO becomes equivalent to the optimization of the forward KL divergence, resembling our Forward SAC algorithm.

However, our Forward SAC algorithm differs from variational policy optimization in two key aspects:

1. The Forward SAC algorithm uses the Q-learning process directly from the SAC algorithm, whereas variational policy optimization employs the E-step to optimize the variational distribution.
2. The Forward SAC algorithm updates the policy by directly learning from the optimal projection, while variational policy optimization utilizes the M-step to optimize the ELBO for policy updating.

Therefore, while there are similarities between our Forward SAC algorithm and variational policy optimization, the updating processes are fundamentally different.

E Broader impacts

Our work on Bidirectional SAC presents several potential positive societal impacts. The improved sample efficiency could significantly reduce the computational resources required for training reinforcement learning agents, thereby lowering energy consumption and associated environmental impacts. Enhanced performance in continuous control tasks may accelerate advances in robotics for healthcare (e.g., assistive devices, surgical robots), industrial automation, and sustainable energy systems. The theoretical insights connecting forward and reverse KL divergence may contribute to the broader field of probabilistic machine learning.

F Experiment details

All environments tested in our experiments are trained for 10^6 steps, except for the Pusher and Lunar Lander environments, which converge fast across all tested algorithms. To leverage GPU acceleration for training and simulation, we use the Brax simulator, which is built on Jax [Freeman et al., 2021]. All experiments are conducted on a cluster server equipped with an NVIDIA RTX A6000 GPU and 32 cores of an Intel(R) Xeon(R) Gold 5218 CPU operating at 2.30 GHz.

F.1 More experiment results in episodic reward

Here we demonstrate more experimental results in MuJoCo and Box2D environments.

The experiment is further extended to more environments as shown in Figure 10. In the Lunar Lander environment, PPO exhibits superior performance by gradually achieving positive rewards, whereas both Bidirectional SAC and traditional SAC struggle to escape negative reward regions. DDPG demonstrates considerable variance but eventually reaches positive performance. For the Inverted Pendulum task, most algorithms converge rapidly to optimal performance, with traditional SAC,

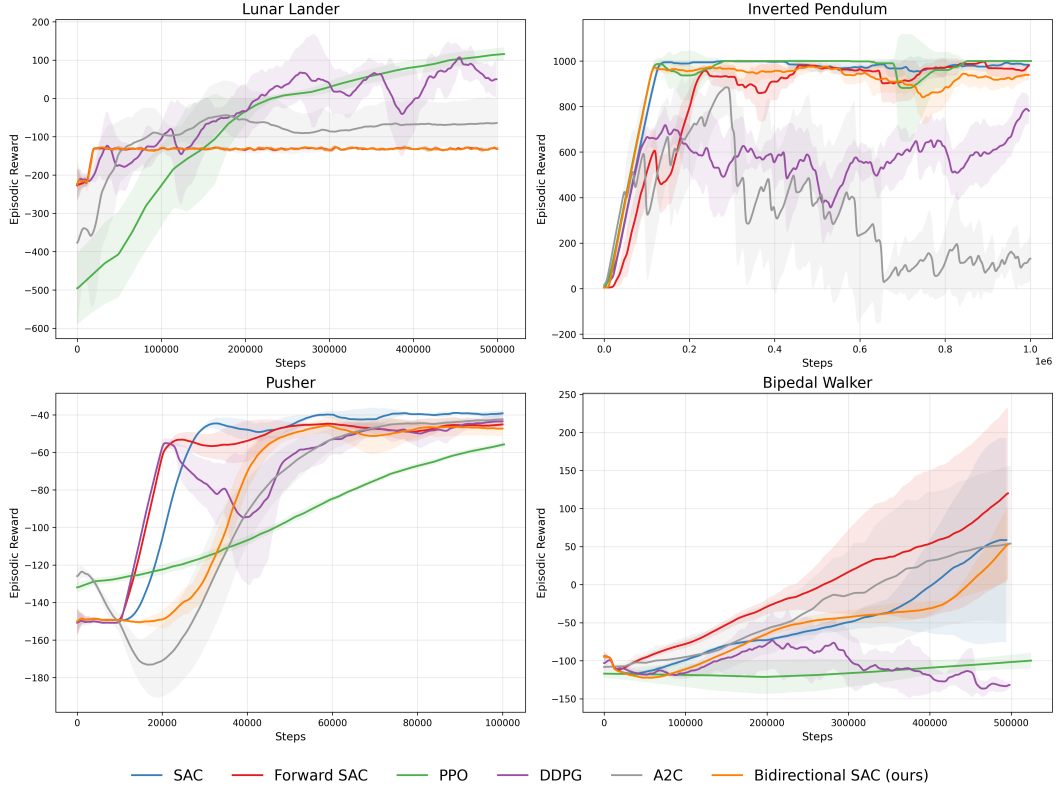


Figure 10: The episodic reward in MuJoCo and Box2D environments for Bidirectional SAC, Forward SAC, and other benchmarks in the training process.

Bidirectional SAC, and PPO maintaining consistently high rewards. Forward SAC experiences some training instability before catching up, while A2C suffers significant performance degradation in later stages. Most notably, in the Bipedal Walker environment, Forward SAC distinguishes itself by attaining the overall best performance.

F.2 More distribution comparison in update steps

